

# Atomic Diagnostics of X-ray Irradiated Protoplanetary Disks

R. Meijerink and A. E. Glassgold

*Astronomy Department, University of California, Berkeley, CA 94720*

rowin@astro.berkeley.edu, glassgol@astro.berkeley.edu

and

J. R. Najita

*National Optical Astronomy Observatory, Tucson, AZ 85719*

najita@noao.edu

## ABSTRACT

We study atomic line diagnostics of the inner regions of protoplanetary disks with our model of X-ray irradiated disk atmospheres which was previously used to predict observable levels of the Ne II and Ne III fine-structure transitions at 12.81 and 15.55  $\mu\text{m}$ . We extend the X-ray ionization theory to sulfur and calculate the fraction of sulfur in S, S<sup>+</sup>, S<sup>2+</sup> and sulfur molecules. For the D'Alessio generic T Tauri star disk, we find that the S I fine-structure line at 25.55  $\mu\text{m}$  is below the detection level of the *Spitzer* Infrared Spectrometer (IRS), in large part due to X-ray ionization of atomic S at the top of the atmosphere and to its incorporation into molecules close to the mid-plane. We predict that observable fluxes of the S II 6718/6732 Å forbidden transitions are produced in the upper atmosphere at somewhat shallower depths and smaller radii than the neon fine-structure lines. This and other forbidden line transitions, such as the O I 6300/6363 Å and the C I 9826/9852 Å lines, serve as complementary diagnostics of X-ray irradiated disk atmospheres. We have also analyzed the potential role of the low-excitation fine-structure lines of C I, C II, and O I, which should be observable by SOFIA and *Herschel*.

*Subject headings:* accretion, accretion disks – infrared: stars – planetary systems: protoplanetary disks – stars: formation – stars: pre-main-sequence – X-rays: stars

## 1. Introduction

There is growing evidence for the existence of warm atmospheres in the inner disks of low and intermediate mass young stellar objects (YSOs). They first became apparent from observations of the CO overtone bandhead emission near  $2.3 \mu\text{m}$  in Herbig Ae stars and T Tauri stars (e.g., Carr 1989; Najita et al. 2000). More recently, the emission from the fundamental CO ro-vibrational band near  $4.6 \mu\text{m}$  has been observed in many T Tauri stars (Najita et al. 2003), as has the UV fluorescence of molecular hydrogen (e.g., Herczeg et al. 2002). These observations indicate that temperatures in the range 1000-2000 K occur over a considerable vertical column density of hydrogen  $\sim 10^{21} \text{ cm}^{-2}$  in the inner disk region. This and other spectroscopic evidence for warm gaseous disk atmospheres were reviewed by Najita et al. (2007), where extensive references are given to earlier work.

Calvet et al. (1991) pioneered the now widely accepted view that disk atmospheres are heated by stellar radiation. In previous publications (Glassgold, Najita & Igea 2004, henceforth GNI04) we argued that stellar X-rays play an important role in heating the upper gas layers of circumstellar disks on the following basis. First, significant X-ray emission appears to be a universal aspect of low-mass YSOs; second, X-rays couple strongly to the gas; and third, hard X-rays with energies  $\gtrsim 1 \text{ keV}$  can penetrate deeply into disk atmospheres.

One special aspect of X-ray irradiation is that temperatures as large as 4000-5000 K are achieved high in the atmosphere. We recently pointed out that this hot layer gives rise to significant flux levels of the fine-structure lines of neon at  $12.81 \mu\text{m}$  and  $15.55 \mu\text{m}$  (Glassgold et al. 2007, henceforth GNI07).

The NeII  $12.81 \mu\text{m}$  line has now been detected in many YSOs by the *Spitzer* Infrared Spectrometer (IRS) in nearby star-forming regions (Pascucci et al. 2007; Lahuis et al. 2007; Espaillat et al. 2007) and by MICHELLE at Gemini North (Herczeg et al. 2007). The measured fluxes are in good agreement with the predictions in GNI07. These observations support the hypothesis that disk atmospheres are heated and ionized by photons energetic enough to ionize Ne (which has first and second ionization potentials of 21.56 and 41.0 eV), most likely X-rays. A key motivation in the work of GNI07 was the search for clear diagnostics of the effects of X-ray irradiation. The Ne lines seemed particularly appropriate because hard X-rays generate high ionization states of neon via the Auger effect and because neon chemistry is especially simple. Gorti & Hollenbach (2006, private communication) have suggested that EUV radiation may contribute to the neon fluxes, although the emission characteristics of YSOs in this wavelength band are poorly known compared to X-rays.

In this paper we extend the considerations of GNI07 and seek other fine-structure and forbidden transitions that have a potential to complement the neon lines. We have been

guided in part by the intrinsic strength of a line, which we can take as the thermalized emissivity in a transition from an upper to a lower level  $u \rightarrow l$ ,

$$j(u, l) = P(u) x n_{\text{H}} A(u, l) E(u, l). \quad (1)$$

Here  $x n_{\text{H}}$  is the density of the emitting species,  $P(u)$  is the population of the upper level, and  $A(u, l)$  and  $E(u, l)$  are the Einstein  $A$ -value and energy of the transition. The last two factors in equation (1) emphasize high frequency transitions, but the other factors are crucial since they require a theory for the ionization of the carrier species (the  $x$  factor) and the excitation of the level (the factor  $P(u)$ ), since they are sensitive to the physical conditions. We have chosen to focus here on the lines of oxygen, sulfur and, to a lesser extent, carbon. Some spectral lines of particular interest are the  $25.25 \mu\text{m}$  fine-structure transition of SI, which has been searched for, mostly without success, by *Spitzer*; the fine-structure lines of OI, which should be detectable with SOFIA and the PACS imaging spectrometer on *Herschel*; and various optical-infrared forbidden transitions accessible from the ground.

The atomic carriers of these lines appear in the many disk chemical models developed over the last 10-15 years (reviewed by Bergin et al. 2007). They are closely related to the photon-dominated models (PDR) developed for the interstellar medium. In this case stellar and interstellar radiation generate warm atomic regions in the upper and lower layers of the disks until the UV radiation is absorbed and molecule formation becomes efficient. Jonkheid and Kamp and their collaborators (Jonkheid et al. 2004, 2006, 2007; Kamp et al. 2003) have gone further and calculated the emissivity and lineshape of the fine-structure lines of CI, CII, and OI.

The  $63 \mu\text{m}$  fine-structure line of OI was detected in YSOs with the KAO (e.g., Cohen et al. 1988; Ceccarelli et al. 1997) and with ISO (e.g., Nisini et al. 1999; Spinoglio et al. 2000; Creech-Eakman et al. 2002; Liseau et al. 2006), but the interpretation of the results is hampered by the low spatial and spectral resolution of the observations so that it is unclear what fraction of the emission arises from the disk. Disks have also been considered as a possible source of forbidden line emission by Hartigan et al. (1995), Kwan (1997) and Störzer & Hollenbach (2000). The forbidden lines have been well studied in YSOs (see, e.g., the review by Ray et al. 2007), and some of the observed “low-velocity-components” of the emission may originate from the disks in these systems (e.g., Kwan & Tadamaru 1988, 1995). We will return to the discussion of the observations of the fine-structure and forbidden lines in Section 5.

The calculations reported in this paper are exploratory in nature, as were those in GNI07. They examine the ability of X-rays, a well characterized property of TTS, to produce atomic line emission from T Tauri disks. The model employs the continuous disk density distribution developed by D’Alessio et al. (1999) for a generic T Tauri star, and they feature

stellar X-ray heating and ionization in the context of a simplified thermal-chemical model, which will be discussed in more detail in Section 2. We do not attempt to fit the observations for any specific system, but instead try to derive conclusions that might be applicable to any protoplanetary disk.

The plan of the rest of this paper is as follows. In the next section, we review and update the thermal-chemical model of GNI04. In Section 3, we summarize the essentials of the basic ionization theory and extend it to include the X-ray ionization of sulfur. In Section 4, we outline the excitation and flux calculations for the lines of interest, and then discuss the relevant observations in Section 5. The last section summarizes the main results of this paper.

## 2. Review Of The Model

We use the thermal-chemical model of GNI04 with minor corrections and updates. The important processes in determining the thermal balance are X-ray heating, gas-grain heating and cooling, mechanical heating (e.g., from disk accretion or the wind-disk interaction), and line cooling ( $\text{Ly}\alpha$ , recombination lines, O I fine-structure and forbidden lines, and CO rotational and ro-vibrational lines). The chemical network contains about 125 reactions and 25 species. Errors in the specification of these processes have been corrected, and the entire reaction base has been re-evaluated and updated. None of the changes affects the conclusions of GNI04 and GNI07 in any major way. GNI04 provide a detailed description of the physical processes, and the chemical reaction base is available from the authors on request or can be downloaded at [http://astro.berkeley.edu/~rowin/MGN\\_rates.pdf](http://astro.berkeley.edu/~rowin/MGN_rates.pdf).

Following GNI04 and GNI07, we calculate the chemical and thermal structure of the gas in a protoplanetary disk for the smooth density distribution of the generic T-Tauri disk model of D’Alessio et al. (1999) using an updated version of the code developed by GNI04. D’Alessio et al. (1999) did not distinguish between the thermal properties of the dust and the gas, and their density structure is in hydrostatic equilibrium. However, at high altitudes and low vertical column densities, the temperature of the gas is much higher than the dust (GNI04), and this implies that our model is no longer in hydrostatic equilibrium. Were we to treat the gas and dust as two separate fluids and require hydrostatic equilibrium, the results would differ somewhat from the exploratory calculations reported here and in GNI07. For example, we would expect the gaseous disk to be puffed up close to the star and to shield the outer part of the disk from stellar radiation. On the other hand, the flaring of the outer disk would also be increased, and thus it would be illuminated more directly by the central star (Dullemond et al. 2002; Gorti & Hollenbach 2004). A quantitative evaluation of such

effects on the diagnostic line fluxes must await the development of a more complete model that treats both the gas and the dust self-consistently.

The D’Alessio model does not include X-rays. In our previous studies based on this density distribution, we adopted a “reference” X-ray luminosity of  $L_X = 2 \times 10^{30}$  erg s<sup>-1</sup> and a thermal spectrum with  $kT_X = 1$  keV. It is well known that both the X-ray luminosity and spectrum of young stellar objects can change with time, and that they vary widely from source to source. The ionization rate is not very sensitive to the temperature of the spectrum, as shown in Fig. 5 of Igea & Glassgold (1999). In the *Chandra* Orion Ultradeep Project (COUP) study of the Orion Nebula Cluster (Getman et al. 2005), the X-ray luminosity function for the entire cluster spans 5 decades from  $\log L_X = 27 - 32$ . Two of these decades of variation may be associated roughly with the dependence of  $L_X$  on stellar mass and one on a dependence on stellar age (Feigelson et al. 2005), leaving two or more unexplained decades. Thus the X-ray luminosity of a pre-main-sequence object with specific mass and age may vary over two orders of magnitude. This is consistent with the findings of Wolk et al. (2005) for a subset of 28 solar-mass stars in the Orion Nebula Cluster with masses in the range  $M_* = 0.9 - 1.2M_\odot$ , which have a median X-ray luminosity of  $\log L_X = 30.25$  erg s<sup>-1</sup>. The spread of two orders of magnitudes can only be partly explained by variability, including flares. Similar results have been found in the XMM-*Newton* study of the Taurus-Aurigae cluster (Güdel et al. 2007; Telleschi et al. 2007), where the X-ray luminosity ranges over three decades ( $\log L_X = 28 - 31$ ).

Our previous choice  $L_X = 2 \times 10^{30}$  erg s<sup>-1</sup> was consistent with the observations of young T Tauri stars with masses  $M_* \sim 1M_\odot$  and with the X-ray luminosity of well studied sources such as TW Hya (Kastner et al. 2002; Stelzer & Schmitt 2004). The median X-ray luminosity measured by XEST for classical T Tauri stars (with disks) in the Taurus-Aurigae cluster is  $L_X = 5 \times 10^{29}$  erg s<sup>-1</sup>, four times smaller than our reference value. In recognition of this difference as well as in the observed 1-2 dex spread in measured luminosity, we will consider a range of X-ray luminosities between  $L_X = 2 \times 10^{29} - 2 \times 10^{31}$  erg s<sup>-1</sup>. X-ray luminosities in this range are likely to yield fluxes for the lines of interest that can be detected with current facilities.

In order to improve the numerical accuracy of the flux calculations in Section 4, the calculations reported here cover an extended range of radii from 0.25-100 AU, in contrast to GNI07 who considered the range 1-40 AU. In making this extension, we do not consider any structural and physical modifications that might occur at very small and very large radii. For example, spectral energy distributions measured with the *Spitzer* IRS indicate the occurrence of inner holes and rims at distances of the order of several AU (Dullemond et al. 2007). Since we use the D’Alessio model calculations, which varies continuously from 0.028

to  $> 500$  AU, the present calculations do not take into account structures such as holes, gaps, and rims.

The elemental abundances used here and in the flux calculations to follow are:  $x_{\text{He}} = 0.1$ ,  $x_{\text{C}} = 2.8 \times 10^{-4}$ ,  $x_{\text{O}} = 6.0 \times 10^{-4}$ ,  $x_{\text{S}} = 7.0 \times 10^{-6}$ ,  $x_{\text{Ne}} = 1.0 \times 10^{-4}$ , and  $x_{\text{Na}} = 1.0 \times 10^{-6}$ . The abundance of sulfur that we have adopted is in the range suggested by the recent modeling of sulfur molecules observed in the Horsehead Nebula (Goicoechea et al. 2006). It is much closer to the solar photospheric/meteoritic value (Asplund et al. 2005) than the heavily depleted values used in modeling dark clouds (e.g., Millar & Herbst 1990). UV absorption line studies of the diffuse interstellar medium provide no evidence for depletion of sulfur, as they do for more refractory elements (Savage & Sembach 1996). Fig. 1 shows the thermal structure of the reference disk model. The stellar and disk parameters that define the D’Alessio 1999 model are given in the caption. For high altitudes ( $N_{\text{H}} < 10^{21} \text{ cm}^{-2}$ ) and moderate radii ( $R < 25$  AU), temperatures as high as 4000-5000 K are reached. Going deeper into the atmosphere,  $T$  undergoes a sharp drop toward mid-plane temperatures in the range from 30 to 200 K, depending on radius. Near the mid-plane, where the density is high ( $n = 10^8 - 10^{10} \text{ cm}^{-3}$ ), the gas and the dust are thermally coupled. For these radii ( $< 25$  AU), the temperature starts high at the top of the atmosphere and then increases further with increasing vertical column density or decreasing altitude (see also Figure 2 of GNI04). This is a consequence of the balance between X-ray heating and Ly- $\alpha$  cooling that controls the temperature at the very top of the atmosphere. The heating and the cooling are both proportional to the first power of the volume density. The small increase in temperature arises from **its** logarithmic dependence on optical depth, which of course increases with increasing vertical column density. Beyond 25 AU, the O I fine-structure lines are the dominant coolants at the disk surface.

### 3. Ionization theory

The GNI07 thermal-chemical program includes the elements H, He, C and O, plus a generic heavy atom represented by Na. X-ray ionization of H, He,  $\text{H}_2$  and C are included explicitly, and that of O implicitly. Generally speaking, X-ray ionization of a cosmic gas occurs by the absorption by the K and L shell electrons of heavy atoms and ions. The resultant photo and Auger electrons then generate many more secondary electrons by the collisional ionization of H and He. The ionization state of a heavy atom A or ion in a mainly atomic gas is determined by several processes: direct X-ray ionization (rate  $\zeta_{\text{dir}}$ ); secondary electron ionization (rate  $\zeta_{\text{sec}}$ ); electronic recombination; and charge transfer to H and He. The latter process may be fast (rate coefficient  $\sim 10^{-9} \text{ cm}^3\text{s}^{-1}$ ) or slow. In the case of neon

(GNI07), charge transfer is relatively slow and fosters high abundances of neon ions. The ionization rates for atom A,  $\zeta_{\text{dir}}(\text{A})$  and  $\zeta_{\text{sec}}(\text{A})$ , are always per atom, whereas the total ionization rate  $\zeta$  is per H nucleus.

On the basis of its elemental X-ray absorption cross section, we estimate that the oxygen ionization rates are  $\zeta_{\text{dir}}(\text{O}) = 17\zeta$  and  $\zeta_{\text{sec}}(\text{O}) = 2.4\zeta$ , where  $\zeta$  is the X-ray ionization rate of the cosmic mix of disk gas. However, near-resonant charge exchange of  $\text{H}^+$  and O is fast and dominates the ionization of oxygen. Thus direct X-ray ionization of oxygen can be ignored, as in GNI04. In the case of carbon, we estimated  $\zeta_{\text{dir}}(\text{C}) = 6\zeta$  and  $\zeta_{\text{sec}}(\text{C}) = 4\zeta$ , but now charge exchange of  $\text{H}^+$  and  $\text{He}^+$  with C is very slow, and therefore X-ray ionization of carbon is important and is included explicitly in the thermal-chemical program.

Figure 2 shows the electron fraction calculated for our model; it exceeds 0.01 at the top of the atmosphere down to a depth of  $N_{\text{H}} \sim 10^{19} \text{cm}^{-2}$ . The electron fraction decreases more smoothly with vertical column than the temperature. Near the mid-plane, its value is larger than that given by GNI07 because ionization due to the radioactive decay of  $^{26}\text{Al}$  have been included at a rate  $\zeta_{26} = 4 \times 10^{-19} \text{s}^{-1}$  (Stepinski 1992; Glassgold 1995; Finocchi & Gail 1997). This assumes that the entire disk is optically thick with respect to the 1.809 MeV decay  $\gamma$ -rays, and that the  $^{26}\text{Al}/^{27}\text{Al}$  ratio has the canonical value found in meteoritic calcium-aluminum inclusions ( $5 \times 10^{-5}$ ). It also ignores the effects of the 1 Myr mean life of  $^{26}\text{Al}$  and the possibility that the initial distribution of  $^{26}\text{Al}$  is spatially inhomogeneous. In light of these simplifying assumptions, it is likely that the rate is even smaller than the one we have adopted, but the exact value is not crucial for the main subject of this work<sup>1</sup>. We use a separate program to obtain the abundances of neon and sulfur species. The ionization calculation of neon is essentially the same as GNI07. Figure 3 shows the fractional abundances of  $\text{Ne}^+$  and  $\text{Ne}^{2+}$  relative to the total abundance of neon. Abundances of the order  $\sim 0.1$  or more are found at high altitudes ( $N_{\text{H}} < 10^{21} \text{cm}^{-2}$ ). It is remarkable that X-ray ionization produces significant abundances of  $\text{Ne}^+$  and  $\text{Ne}^{2+}$  out to radii as large as 30 AU.

The closed shell character of neon means that the complexities of molecule formation and destruction do not enter, and only three species, Ne,  $\text{Ne}^+$  and  $\text{Ne}^{2+}$  have to be considered in estimating their line fluxes. This is not the case for the calculation of the SI and SII fine-structure and forbidden lines. In order to calculate the abundances of S and  $\text{S}^+$ , we have to consider the transition into sulfur molecules, such as SO,  $\text{SO}_2$  and CS, which occurs at large vertical column densities. Figure 4 gives a schematic overview of sulfur ionization

---

<sup>1</sup>Many modelers of disk chemistry have used  $^{26}\text{Al}$  ionization rates an order of magnitude larger than we have as the result of a typographical error in the paper by Umebayashi & Nakano (1981).

including a simplified warm chemistry, following Leen & Graff (1988).

Sulfur ions in the disk are mainly produced by X-ray ionization. Sulfur has L and K edges near 0.2 and 2.5 keV and, since we consider X-ray spectra that are not particularly hard ( $T_X \gtrsim 1$  keV), photons with energies between the L and K edges are the ones most strongly absorbed by sulfur. Because charge exchange with H is fast for highly-ionized sulfur ions, X-ray ionization of sulfur accompanied by the Auger process leads primarily to  $S^{2+}$  and  $S^{3+}$ . Calculations by Butler & Dalgarno (1980) and Christensen & Watson (1981) suggest that  $S^{3+}$  charge exchange with atomic hydrogen is also fast, while that of  $S^{2+}$  is slow. Therefore, we only include ions up to  $S^{2+}$ , as we did in the case of neon (GNI07). However, in addition to electronic recombination and charge exchange of sulfur ions with atomic hydrogen, we also include the  $S + H^+$  charge-exchange reaction, which can ionize S at a significant rate below 10000 K according to the theoretical calculations of Zhao et al. (2005). Furthermore, the reaction  $S^{2+} + H_2$ , which has been measured to be fast (Chen et al. 2003), can significantly reduce the abundance of  $S^{2+}$ .

As for carbon and oxygen, we can estimate the direct X-ray ionization rate of sulfur from its X-ray absorption cross section. Its energy dependence is very similar to that of the mean X-ray absorption cross section averaged over interstellar or solar abundances. Thus the direct ionization rate of sulfur, resulting from the (L to K) 0.2-2.4 keV band is basically given by the ratio of the two absorption cross sections at these energies. For example, at 1 keV, the ratio is  $\approx 500$ . This then is the approximate ratio of the primary or direct X-ray ionization of sulfur (per sulfur nucleus) to that of the mean interstellar atom (per hydrogen nucleus, since abundances are conventionally normed to hydrogen). However, most of the ionization of the gas as a whole comes from secondary-electron ionization of hydrogen (atomic and molecular) and helium. Since there are roughly 25 such electrons produced per primary ionization, the ratio of the direct sulfur ionization rate per sulfur nucleus to the total X-ray ionization per H nucleus is  $500/25 = 20$ :

$$\zeta(S)_{\text{dir}} \simeq 20\zeta. \quad (2)$$

The secondary electrons generated by X-ray ionization of all of the cosmic elements collisionally excite and ionize S at a rate that is roughly given by the ratio of the electronic ionization cross section of sulfur to that of hydrogen (Maloney et al. 1996). This leads to the approximate value,

$$\zeta(S)_{\text{sec}} \simeq 5\zeta. \quad (3)$$

The direct ionization rate is mainly responsible for producing higher S ions, which we lump together into  $S^{2+}$  because of fast charge transfer. The secondary ionization rate primarily produces an additional electron, e.g., it generates  $S^+$  from S. Some of the sulfur ion rate coefficients are listed in Table 1. Those for radiative recombination are well calculated. As



in the case of neon, however, the rate coefficients for electron transfer from atomic hydrogen are not well established. They represent an important uncertainty in the results of this paper.

To address the question of whether S remains the dominant species near the mid-plane, we include the formation and destruction of the sulfur molecules, SO, SO<sub>2</sub>, CS and OCS, by using the warm neutral sulfur chemistry of (Leen & Graff 1988). We also include X-ray ionization and destruction of these molecules, assuming that X-ray cross sections for molecules are additive over the constituent atoms, and using the atomic rates discussed above. We also make the simplifying assumptions that a direct absorption of an X-ray by a sulfur molecule always leads to dissociation, and that secondary electronic ionization always produces a molecular ion. The sulfur molecular ions are rapidly destroyed by dissociative recombination. The branching ratios are summarized by Florescu-Mitchell & Mitchell (2006).

Figure 5 shows the fractional abundances of the sulfur species S<sup>+</sup>, S, SO<sub>2</sub> and CS as a function of vertical column density above the disk mid-plane at a radial distance of 20 AU from the star. We find that sulfur is completely locked up in molecules for column densities larger than  $0.5-1.0 \times 10^{22} \text{ cm}^{-2}$ . In this region, neutral formation reactions start to dominate over X-ray destruction as the X-rays get shielded and the increased density enhances the reaction rates. The main species at large column densities is SO<sub>2</sub>, but there may also be a layer of CS at intermediate column densities.

Figure 6 shows the S and S<sup>+</sup> fractions relative to the total abundance of sulfur in the disk for radii between 0.25 and 40 AU. S<sup>+</sup> is the dominant species at the highest altitudes for  $R < 25 \text{ AU}$ , whereas S assumes that role at intermediate altitudes. Beyond  $R > 25 \text{ AU}$ , X-ray ionization of sulfur is not strong enough to maintain S<sup>+</sup> as the dominant species. At low altitudes, we find a clear cut-off in the atomic S abundance, with almost all of the sulfur in molecules.

#### 4. Excitation and Flux Calculations

The flux calculations for the atomic ions considered in this paper are relatively straightforward because one needs to deal only with a few levels of relatively low excitation, even for the forbidden lines. For neon, we continue to focus on the ground fine-structure transitions of Ne<sup>+</sup> and Ne<sup>2+</sup>. For O, S and C, we treat the 5 lowest levels in the ground electronic configuration: a fine-structure triplet, that produces mid and far IR lines, and two higher-energy singlet levels that give rise to forbidden optical-IR transitions. For C<sup>+</sup>, we consider only the ground level fine-structure doublet that generates the famous  $158 \mu\text{m}$  line. Simpli-

fications often occur. For example, the fine-structure transitions of CI and CII have low critical densities and, because of the high disk densities, are near-thermalized. Similarly, the forbidden lines are usually optically thin and the effects of line trapping are small. In the following sections, we discuss specific issues that arise in the calculation of the emissivities of the lines of interest. We use the line frequencies and  $A$ -values in the NIST data base (<http://physics.nist.gov/PhysRefData/ASD/index.html>). Electronic excitation rates are now reasonably well established, but those for excitation by H, H<sub>2</sub>, He and H<sup>+</sup> are often unknown, except perhaps for OI, CI and CII. References for our choice of rate coefficients are given in Table 2. In those cases where trapping plays a role, e.g., for the OI and SI fine-structure lines, our results apply to a face-on disk.

#### 4.1. Neon

We calculate the optically-thin NeII and NeIII lines fine-structure lines at 12.81 and 15.55  $\mu\text{m}$  in the manner of GNI07 with the following change. While retaining the two-level population formula for the ground-level doublet of Ne II, we solve exactly for the populations of the ground-level triplet of Ne III<sup>2</sup>. This more complete excitation calculation leads to an increase in the population of the upper  $J = 0$  level and, to a lesser extent, the  $J = 1$  level, and increases the line intensities.

Figure 7 shows the distribution of the NeII 12.81  $\mu\text{m}$  emissivity throughout the disk for the reference X-ray luminosity. Most of the emission is produced at high temperature ( $\sim 4000$  K) and high electron abundance, corresponding to radial distances  $R < 25$  AU and vertical column densities  $N_H < 10^{21}$  cm<sup>-2</sup>. The largest emissivity does not always occur at the highest altitude above the mid-plane. This is due to an increase of the Ne<sup>+</sup> density and its specific emissivity with increasing depth. The upper  $J = 1/2$  level is sub-thermally populated and its population is proportional to the electron density, which also increases going down into the atmosphere.

The above calculations assume that the excitation is solely due to electronic collisions. However, we have been reminded that, as the electron fraction decreases with height, collisions with atomic hydrogen begin to play a role (D. J. Hollenbach 2006, private communi-

---

<sup>2</sup>GNI07 omitted the weak quadrupolar transition that connects the top ( $J = 0$ ) and bottom ( $J = 2$ ) levels. Their approximate equation (3-4) also contained a typo; the correct formula is,

$$P_u(2) = \frac{1.0}{1 + 5/3C_{1-2} \exp 925.3/T + 1/3 \exp(-399/T)/C_{0-1}} \quad (4)$$

cation). Using the results of Bahcall & Wolf (1968), Hollenbach & McKee (1989) estimated the rate coefficient for the de-excitation of the  $12.81\ \mu\text{m}$  transition in collisions with atomic hydrogen to be  $1.3 \times 10^{-9}\ \text{cm}^3\ \text{s}^{-1}$ . Although the theory of Bahcall and Wolf may give the right order of magnitude (as it does for the excitation of the O I fine-structure transitions), it is incorrect in principle since it implies that the excitation cross section is proportional to the scattering cross section. According to Bahcall and Wolf, the rate coefficient in a collision with a neutral atom varies with temperature as  $T^{1/6}$  (c.f. the van der Waals potential) and as a constant in a collision with an ion (c.f. the Langevin potential). However, collisional excitation of a fine-structure transition requires an exchange of a spin between the incident H atom and the target electrons and thus depends on differences between potentials, differences which decrease more rapidly than  $1/r^6$  and  $1/r^4$  for neutral and ionic collisions, respectively.

The full quantum-mechanical calculations for O I and C I (Launay & Roueff 1977a; Abrahamsson et al. 2007) and for C II (Launay & Roueff 1977b; Barinovs et al. 2005) bear out the fact that the Bahcall and Wolf theory predicts the wrong temperature dependence for the collisional excitation rate coefficients by atomic hydrogen. We have compared the recent calculations of Barinovs et al. (2005) for  $\text{H} + \text{C II}$  with the Bahcall and Wolf theory, and find that the latter over-estimates the rate coefficient by factors of 7.5 to 5 in the temperature range from 500-4000 K. If something like this reduction factor also applies to  $\text{H} + \text{Ne II}$ , then the order of magnitude of its rate coefficient for collisional de-excitation of the Ne II fine-structure doublet is  $\sim 2 \times 10^{-10}\ \text{cm}^3\ \text{s}^{-1}$ . We have calculated the  $12.81\ \mu\text{m}$  emissivity (including line trapping) with this value for the H de-excitation rate, and find that it increases the flux by about a factor of two. This increase arises mainly at large radial distances, where the deviations from a thermal population are the greatest. We conclude that our calculations based on electronic excitation alone underestimate the Ne II  $12.81\ \mu\text{m}$  flux, but possibly not by a large factor. Actual calculations of the atomic hydrogen excitation rate would be most welcome.

## 4.2. Oxygen

Figure 8 gives the 5 levels that we consider in calculating fine-structure and forbidden line emission from atomic oxygen and sulfur. According to Table 2, collisional excitation rates for the fine-structure levels of O I are available for collision partners e, p, H,  $\text{H}_2$  and He. Atomic hydrogen tends to dominate and, even without line trapping, the critical densities are modest, typically  $n_{\text{cr}}(\text{H}) < 10^6\ \text{cm}^{-3}$ . At radii ( $> 25\ \text{AU}$ ), densities of this order are not reached until vertical column densities  $N_{\text{H}} \approx 10^{20} - 10^{21}\ \text{cm}^{-2}$ . The full emissivity calculation is particularly relevant at large radii.

Figure 9 shows the spatial distribution of the emissivity of the O I  $63\ \mu\text{m}$  fine-structure line. The results for the O I  $146\ \mu\text{m}$  line (not shown) are similar. The spatial profile is particularly complicated at small radii ( $< 10\ \text{AU}$ ). The emissivity has two peaks going down into the disk (increasing vertical column at fixed radius) that result from a combination of effects: density and temperature variations, abundance changes and line-trapping. The declining temperature, the conversion of atomic oxygen into molecules (CO,  $\text{H}_2\text{O}$  and  $\text{O}_2$ ), and trapping at large columns all tend to decrease the emissivity. These effects are illustrated by Figure 10, which shows the *specific emissivity* (per O atom). For small column densities, it is constant when the population is thermalized (at radii  $R < 10\ \text{AU}$ , where the critical densities are reached), or it increases toward a maximum when the critical densities are only attained at larger vertical column densities. Then it decreases again with vertical column density, except at the smallest radii ( $< 1\ \text{AU}$ ), where the rise in temperature due to viscous heating close to the mid-plane has the opposite effect. The occurrence of the two peaks in emissivity at intermediate columns is the result of the rapid increase of volumetric density with increasing depth. Significant emission occurs beyond columns of  $N_{\text{H}} = 10^{22}\ \text{cm}^{-2}$  as a consequence of the fact that the excitation energy is relatively low ( $\approx 230\ \text{K}$ ) and contributes  $\sim 10\%$  of the total line flux.

The  $^1D_2 - ^3P_J$  O I  $6300/6363\ \text{\AA}$  and the  $^1S_0 - ^1D_2$   $5577\ \text{\AA}$  forbidden transitions are optically thin and sub-thermally excited. In addition to the electronic rate coefficients (Zatsarinny & Tayal 2003), the collisional de-excitation rate of the  $^1D_2$  level by atomic hydrogen has been calculated by Křems et al. (2006). It varies little between 500-6000 K, where it has a mean value of  $8 \times 10^{-13}\ \text{cm}^3\ \text{s}^{-1}$  to within 25%. At 4000 K, the collisional electron de-excitation rate is  $3 \times 10^{-9}\ \text{cm}^3\ \text{s}^{-1}$  for the  $^1D_2$  level, so electronic collisions dominate over those with atomic hydrogen for  $x_e > 2.5 \times 10^{-4}$ . If we consider only electronic collisions, then an upper limit to the critical density for the  $6300/6363\ \text{\AA}$  transitions is  $n_e \approx 10^6\ \text{cm}^{-3}$ , while that for the  $5577\ \text{\AA}$  transition is  $n_e \approx 10^8\ \text{cm}^{-3}$ . In the absence of calculations for the  $^1S_0$  level, we have adopted the value,  $10^{-12}\ \text{cm}^3\ \text{s}^{-1}$ , for the H rate coefficient. Thus the  $6300$  and  $6363\ \text{\AA}$  lines are populated near-thermally, and we can use the two-level formulae given in equations (3-2) and (3-3) of GNI07 that allow for the effects of finite values of the critical density. The emissivity for both lines is then given by equation 1. The  $^1S_0$  uppermost level is so far from being thermalized that we can calculate the flux of the  $5577\ \text{\AA}$  line by using the extreme low-density collisional-excitation limit, in which every excitation leads to the production of a photon.

Figure 11 shows that the O I forbidden lines trace the upper atmosphere of the disk, where the atomic oxygen abundance is constant. The O I  $6300/6363\ \text{\AA}$  lines are generated within 25 AU, a somewhat smaller range than the neon fine-structure lines, while the  $5577\ \text{\AA}$  line (not shown) originates from radii inside 15 AU. These calculations of forbidden line

fluxes necessarily ignore an effect of the UV photodissociation of OH, which leads to significant branching to the excited  $^1D_2$  level of O, producing fluorescent emission of the O I 6300/6363 Å lines (Störzer & Hollenbach 2000). Because significant OH abundances only occur at large depths in our model, this effect might become important at large radii due to OH photodissociation by the stellar or interstellar/intracluster FUV radiation field.

### 4.3. Sulfur

We focus on the mid-IR fine-structure lines of S I and the 6718/6732 Å forbidden transitions of S II; the fine-structure lines of S III are likely to be too weak to be observable at the present time. In accord with Figure 8, the calculation of the S I fine-structure emission is similar to that just described for O I. The big difference is that little is known about the excitation of these lines by collision partners other than electrons. Thus the present flux estimates are lower limits. The calculations take line trapping into account and solve the three-level fine-structure population problem exactly, including the weak  $J = 0 - 2$  quadrupolar transition.

Figure 12 shows the spatial distribution of the S I 25.25  $\mu\text{m}$  fine-structure line emissivity for the reference model. The appearance of the 56.33  $\mu\text{m}$  emissivity (not shown) is similar, but it is concentrated toward smaller radii and higher altitudes. As in the case of O I, the variation of the fine-structure emission with depth at fixed radius is non-monotonic, and again there are several factors that contribute to this behavior. First, there are the chemical changes already mentioned, where sulfur changes from  $\text{S}^+$  to S at high altitudes and from S to sulfur molecules at low altitudes. Thus the emission peaks at intermediate altitudes, at a vertical column of  $N_{\text{H}} \sim 10^{21} \text{ cm}^{-2}$  at  $R = 0.25 \text{ AU}$  and near  $N_{\text{H}} \sim 10^{19} \text{ cm}^{-2}$  at  $R = 25 \text{ AU}$ . Second, the increase of volumetric density with depth also promotes fine-structure emission, whereas the overall temperature decrease has the opposite effect. Figure 13 shows the variation of the specific emissivity with vertical column at fixed radius. For radii in the range 1-25 AU, the emissivity per S atom of the  $J = 1 - 0$  level changes from sub-thermal to thermal as the density increases with increasing depth. At somewhat larger column densities, the specific emissivity decreases due to decreases in both temperature and electron density.

The transition of atomic sulfur into molecules such as SO and  $\text{SO}_2$  has little effect on the absolute level of the S I fine-structure emission. This is due to the fact that electronic excitation has already become ineffective for  $N_{\text{H}} < 10^{22} \text{ cm}^{-2}$  before molecule formation occurs. In order to gauge the importance of H atom collisions, we carried out a calculation where we assumed that the S I fine-structure de-excitation rates are about the same as for O I, specifically  $k(\text{H}) = 5.0 \times 10^{-11} T^{0.4}$  for all transitions. The S I 25.25 and 56.33  $\mu\text{m}$

emission is then increased by factors of 10 or more over that for electron collisions only. This serves to indicate the importance of extending the calculation of H excitation rates to heavy atoms and ions such as NeII and SI.

We estimate the emission of the S II forbidden lines in the optically thin approximation. We concentrate on the  ${}^2D_{5/2,3/2} - {}^4S_{3/2}$  transitions with wavelengths near 6700 Å. Using the electron collisions strengths from Tayal (1997), we find electron critical densities,  $n_{\text{cr}} \sim 10^4 - 10^5 \text{ cm}^{-3} \text{ s}^{-1}$ , and conclude that the lines are almost thermalized. We also considered the possible role of the  $\text{H}^+ + \text{S} \rightarrow \text{S}^+ + \text{H}$  charge exchange, which mainly branches to the upper  ${}^2P_J$  level of  $\text{S}^+$ , and then decays with the emission of photons with wavelengths near 4070 Å, 6700 Å, and  $1 \mu\text{m}$ . We find that this process does not increase the 6718 and 6732 Å line emissivities, probably because the rate coefficient for charge exchange is small ( $\sim 5 \times 10^{-12} \text{ cm}^3 \text{ s}^{-1}$ ) and because the high density tends to thermalize the level population. In Figure 14, we show the emissivity of S II 6718 Å line (the 6733 Å line is very similar). These lines trace the warm upper layers of the disk. Significant emission arises only from regions with temperatures in the range 2000-5000 K.

#### 4.4. Carbon

The energy levels of the ground configuration of CI are similar to those of OI and SI shown in Figure 8, except that the scale of the energy level separations is reduced and the ordering of the total angular momentum quantum number  $J$  in the ground state triplet is inverted. The upper fine-structure levels have energies  $E_2/k = 62.5 \text{ K}$  and  $E_1/k = 23.62 \text{ K}$  and give rise to far-infrared lines with wavelengths  $\lambda(1-0) = 609.135 \mu\text{m}$  and  $\lambda(2-1) = 370.144 \mu\text{m}$ . In addition to these lines, we calculate the emissivity of the forbidden lines at 9827 and 9853 Å that emanate from the first  ${}^1D_2$  level of CI above ground. For CII, we only consider the fine-structure doublet, with excitation energy and wavelength,  $\Delta E(3/2 - 1/2)/k = 91.2 \text{ K}$  and  $\lambda(3/2 - 1/2) = 157.7 \mu\text{m}$ , and ignore the 2300 Å lines that arise from the next  ${}^4P$  level.

The  $A$  values of the CI and CII fine-structure transitions are very small ( $\sim 10^{-7} \text{ s}^{-1}$  for CI and  $2.3 \times 10^{-6} \text{ s}^{-1}$  for CII), which implies that the critical densities for all of these transitions are low ( $< 10^4 \text{ cm}^{-3}$ , based on the collisional rate coefficients referenced in Table 2). Thus we can estimate the emissivities assuming that the fine-structure levels are in thermal equilibrium (but we do include line-trapping). The integrated fluxes for a nominal distance of 140 pc are given in Table 3. The flux of the CII  $158 \mu\text{m}$  line is very small, but the  $369 \mu\text{m}$  line of CI appears to be in the observable range, as may even be the case for the  $609 \mu\text{m}$  line.

We estimate the the CI 9827 and 9853 Å forbidden line emission in the optically thin approximation. Using Table 2, the critical density of the  $^1D_2$  level at 4000 K is  $1.96 \times 10^4 \text{ cm}^{-3} \text{ s}^{-1}$ , and the level is close to being thermalized. The density-dependent correction for sub-thermal excitation is made in the same way as for O I, as described in Section 4.2. The spatial distribution of the CI 9827 Å emission is shown in Fig. 15. The emission is peaked at small vertical column densities, much like the O I 6300 Å emission in Fig. 11. The integrated line flux given in Table 3 is somewhat smaller than the flux of the O I 6300 Å line, but still in the potentially observable range. Of course all of these statements about the detectability of neutral carbon lines stand to be corrected (and reduced) when interstellar/intracluster UV radiation is included in the ionization theory.

## 5. Discussion

In this section we discuss the most important results of this paper in the context of both existing and prospective observations. We treat high and low excitation lines separately, since they trace different parts of the disk. We first summarize in Table 3 the line fluxes for five values of the stellar X-ray luminosity that range from  $L_X = 2 \times 10^{29} - 2 \times 10^{31} \text{ erg s}^{-1}$ . To ensure accurate results for values of  $L_X$  larger than standard, we have calculated the disk properties and emissivities out to 100 AU. The calculations pertain to the case where X-ray heating of the disk atmosphere dominates mechanical heating ( $\alpha_h = 0.01$  in the notation of GNI04). As discussed in Section 2, the underlying density model is the generic T Tauri disk model of D’Alessio et al. (1999); the parameters for the model are given in the caption of Fig. 1. The “reference” model that we have used throughout has an X-ray luminosity of  $L_X = 2 \times 10^{30} \text{ erg s}^{-1}$ ; the fluxes for this case are given in the middle column of the Table.

The values shown in the other columns illustrate how sensitive the modeling results are to the choice of X-ray luminosity. Table 3 encompasses a range of 100 in X-ray luminosity, which is roughly the spread seen by the COUP and XEST projects for T Tauri stars in the Orion Nebula and Taurus-Aurigae clusters of the same mass and age. Were we to choose the median  $L_X$  for Taurus-Aurigae (Telleschi et al. 2007) for the reference model, the second column of fluxes would be appropriate. According to the discussion in the previous sections, all of the flux estimates are themselves uncertain to varying degrees due to uncertainties in the rate coefficients and other limitations of the model. In particular, the fluxes for the neon and sulfur fine-structure lines are lower limits because of the omission of collisional excitation by H atoms.

The sensitivity of the integrated line fluxes to the X-ray luminosity can vary from one line to another, since they may originate in different parts of the disk with different physical

properties. We illustrate this in Fig. 16, which shows how some of the line fluxes vary with  $L_X$ , normalized to the standard model. The CI 369  $\mu\text{m}$  line luminosity depends very weakly on  $L_X$ , since most of the emission is produced at intermediate column densities ( $N_{\text{H}} \sim 10^{22} \text{ cm}^{-2}$ ) where the X-ray flux is strongly attenuated. The OI 63  $\mu\text{m}$  luminosity shows a somewhat steeper dependence, because it is produced both at high altitudes, where the X-ray flux is large, and close to the midplane, where the X-ray flux is small (and the gas and dust temperatures are almost the same). The optically thin OI 5577  $\text{\AA}$  emission displays the strongest dependence on  $L_X$  because, with its relatively high excitation temperature, it is only produced in the warmest part of the disk fully exposed to stellar X-rays. The other forbidden lines and the SI fine-structure lines (not shown), behave very much like the NeII fine-structure line. The almost linear relation between NeII line flux and  $L_X$  arises from the dependence of the emissivity on  $n_e^2$  (c.f. Eq. 4-1 of GNI07). In its present form, Fig. 16 is *not* meant to suggest a general empirical correlation of line fluxes with X-ray luminosity, simply because the stellar and disk properties of the reference model have been held fixed in the calculations for this figure.

## 5.1. High excitation lines

### 5.1.1. Neon Fine-Structure Lines

The neon fine-structure line fluxes (Table 3) are close to but more accurate than GNI07. The Ne III flux is 40% larger since the calculations extend to smaller radii ( $R = 0.25 \text{ AU}$ ). The NeII 12.81  $\mu\text{m}$  line emission arises from the top of the atmosphere, where the temperature and electron density are high. We find significant contributions to the integrated emission out to  $R = 25 \text{ AU}$ . The emissivity per unit radius is determined by the column density in the upper level (c.f. Eq. 3-7 of GNI07). This quantity is plotted in the upper panel of Fig. 17 against the radius  $R$ . In contrast to Fig. 4 of GNI07, there is no dip near 5 AU, thanks to more accurate and closer spaced calculations. When we assume Keplerian rotation to convert from column density to a velocity distribution function  $P(v)$  (c.f. Eq. 3-8 of GNI07), the peak in  $P(v)$  occurs at  $v = 0.25v(1 \text{ AU})$ , which corresponds to a peak in the emissivity per unit area at 16 AU. The bottom panel of Fig. 17 shows that  $P(v)$  has a long tail extending to high velocity. The ratio of the Ne III 15.55  $\mu\text{m}$  to the NeII 12.81  $\mu\text{m}$  flux is of order 0.1. GNI07 considered the detection of the Ne III line to be a near definitive diagnostic of X-ray ionization of neon. However, using a disk model dominated by stellar EUV radiation, Hollenbach & Gorti (2007, private communication), find a range of possible NeIII/NeII ratios (0.1-6) depending on the the nature of the EUV spectrum. Thus it is not immediately clear whether the Ne III/NeII fine-structure line ratio can serve as a discriminant between EUV



and X-ray irradiation.

The NeII 12.81  $\mu\text{m}$  line has now been detected in T Tauri disks in about 20 cases from the ground and from space (by the IRS on *Spitzer*: Pascucci et al. 2007; Lahuis et al. 2007; Espaillat et al. 2007; and MICHELLE on Gemini North: Herczeg et al. 2007). The detected flux levels are of order  $10^{-14}$  erg cm $^{-2}$  s $^{-1}$ ; they are within a factor of few agreement with our model calculations. The weaker 15.55  $\mu\text{m}$  of NeIII line has been tentatively detected in only one case (Sz 102, Lahuis et al. 2007). Based on the  $3\sigma$  detection of the NeIII line, the NeIII/NeII ratio is  $\approx 0.06$ , which might be compared with a ratio  $\sim 0.1$  derived from Table 3. Perhaps what is most interesting about this T Tauri star is that it has the second brightest NeII line detected in the Lahuis et al. survey. Its flux is an order of magnitude larger than the value for our reference model, after correction for the distance of 200 pc. Detailed modeling of the disk around this star would be of considerable interest. For the case of nearby TW Hya, Herczeg et al. (2007) measure the luminosity for the Ne II 12.81  $\mu\text{m}$  line to be  $4.8 \times 10^{-6} L_{\odot}$ , which is 20% larger than the result for our reference model in Table 3.

From a small number of detections of the NeII 12.81  $\mu\text{m}$  line the *Spitzer* Legacy program, “Formation and Evolution of Planetary Systems” (FEPS), Pascucci et al. (2007) have suggested that a linear correlation may exist between the NeII and X-ray luminosities. Together with their detection of the NeII line in CS Cha and that for TW Hya, based on data obtained by Uchida et al. (2004), Espaillat et al. (2007) argue against such a correlation. The range of  $L_X$  in these papers is small, 1.5 for Pascucci et al. (2007) and 2.25 for Espaillat et al. (2007), the same order of magnitude as the observed variability in the X-ray luminosity. Aside from the intrinsic difficulty of deducing a meaningful correlation on the basis of a small dynamical range in YSO X-ray luminosity, it is important to keep in mind that the line fluxes depend on many other stellar and disk properties, e.g., the stellar temperature, mass, and age and the disk mass, accretion rate, and the amount of dust grain growth and settling. The theoretical calculations shown in Fig. 16 may not be relevant in this context because they assume that the disk structure is fixed while  $L_X$  is varied. To pursue the question of the existence of a correlation with  $L_X$ , T Tauri stars with similar properties, both stellar and disk, should be considered. A more practical approach might be to focus in depth on a few specific cases with well observed properties and to use observed X-ray spectra.

Using the MICHELLE spectrometer at Gemini North, Herczeg et al. (2007) have obtained a spectrally resolved NeII line profile for TW Hya, which has a nearly face-on disk. The line is centered at the stellar radial velocity, consistent with a disk origin, but the line is broad with FWHM of  $\sim 22$  km s $^{-1}$ . The rotational broadening in our models (Fig. 5 of

GNI07 and Fig. 17 of this paper), when corrected for inclination, cannot explain the observed line width, even though the present calculations extend to radii as small as 0.25 AU. Although our calculations agree with the measured NeII luminosity, the rotational broadening in the model is small because it arises from relatively large radii, as shown in Fig. 17. As discussed by Herczeg et al. (2007), two interesting explanations of the line width seen TW Hya that deserve consideration are transonic turbulence and photo-evaporative outflows from the disk (Hollenbach et al. 2000; Font et al. 2004). These possibilities raise interesting challenges for future research. If the hole is produced by photo-evaporation, then the wind itself will generate line emission. Furthermore, the inner rim of the hole will be irradiated more or less directly by the star, as in the model of Chiang & Murray-Clay (2007), again producing characteristic line emission.

### 5.1.2. Sulfur Fine-Structure Lines

We consider the SI fine-structure lines to be “high-excitation” because the associated excitation energies, 476 K and 825 K, are larger than the temperatures characteristic of the outer disk, as are the fine-structure levels of the neon ions. As discussed in Section 3, the X-ray ionization theory for neon and sulfur, where charge exchange plays an important role, are also similar. Reference to Table 3 shows that the integrated SI fine-structure emission for our reference model is  $\sim 20$  smaller than for the NeII line. Fig. 12 shows that the strongest emission of the SI 25.25  $\mu\text{m}$  line comes from a relatively thin layer between  $N_{\text{H}} = 10^{19} - 10^{21} \text{ cm}^{-2}$  for  $R < 10 \text{ AU}$ . This situation and the attendant weakness of the 25.25  $\mu\text{m}$  line occur because sulfur is in the form of  $\text{S}^+$  at higher altitudes and electronic excitation becomes weak at lower altitudes (c.f. Figs. 5 and 6).

The SI 25.25  $\mu\text{m}$  line was not detected by the *Spitzer* c2d and FEPS teams. Pascucci et al. (2007) put upper limits on the residual gas in the disks around their survey of older T Tauri stars with ages between 5 and 100 Myr using the model calculations of Gorti & Hollenbach (2004). From Table 3, which is based on pure electronic excitation, the SI fine-structure lines from younger T Tauri disks would be similarly difficult to detect. However, if the atomic H collision rates for SI are similar to those for OI, the predicted fluxes would approach the observable range. It is important to recall several other caveats that pertain to our calculations: the uncertainties in sulfur chemistry, the total abundance of gaseous sulfur in disks, and the poorly known charge-exchange rate coefficients.

### 5.1.3. Forbidden Lines

Table 3 gives the fluxes for our reference model of a sample of forbidden lines, as calculated in Section 4: O I 6300/6363 Å, O I 5577 Å, S II 6718/6731 Å; C I 9827/9853 Å. We have identified them as potential diagnostics of the warm and highly-ionized gas produced by X-ray irradiation in the upper atmosphere of the inner disk. These lines are generated within the same radial distance range as the Ne II 12.81 and 15.55  $\mu\text{m}$  lines, but at somewhat higher elevations. In principle, they can provide complementary checks on our picture of X-ray irradiation. As discussed in Section 4, the accuracy of the calculations varies somewhat from line to line, depending on the reliability of the atomic data and on the completeness of the model itself. For example, we have ignored the role of stellar or interstellar/intracluster FUV radiation, which could enhance the ionization of carbon at high altitudes and thereby reduce the amount of neutral carbon and the strength of the C I forbidden lines. Similarly, the S II 6718 Å line strength is affected by the sulfur atoms being converted into molecules. With this proviso, we can see from Table 3 that many of the forbidden lines generated in the upper disk atmosphere are observable in nearby star-forming regions such as Taurus-Aurigae in the sense that the predicted fluxes are  $\gtrsim 10^{-15} \text{erg cm}^{-2} \text{s}^{-1}$ , notably O I 6300/6363 Å, C I 9827/9853 Å, and perhaps S I 6718/6733 Å.

Many of these lines have been measured in T Tauri stars. The most dramatic manifestation of the forbidden lines is their tracing of high-velocity outflows or jets from YSOs (e.g., Ray et al. 2007). But these flows have a low-velocity as well as a high-velocity component (Kwan & Tademaru 1988, 1995; Hirth et al. 1997). Kwan (1997) suggested that the low velocity component (LVC) originates in the inner regions of T Tauri disks ( $R < 2 \text{AU}$ )<sup>3</sup>. Other possible sources for the origin of the LVC is a MHD disk wind (e.g., Pudritz et al. 2007) or a photoevaporative outflow (e.g., Hollenbach et al. 2000; Font et al. 2004).

Hartigan et al. (1995) have obtained extensive data on forbidden line emission from T Tauri stars. The LVC is ubiquitous, with a typical line luminosity of  $\sim 10^{-4} L_{\odot}$ , an order of magnitude larger than the luminosity of our reference model,  $8.0 \times 10^{-6} L_{\odot}$ . They also find O I 5577 Å to O I 6300 Å line ratios in the range  $\sim 0.2 - 0.5$ ; our model predicts  $\sim 0.1$ . These numbers may signify the difficulty of applying our X-ray irradiated disk model to observations such as the optical forbidden lines that are sensitive to the other dynamic entities that are operative in accreting young stars, e.g., the various flows that arise near the inner edge of the disk. Hartigan et al. define the LVC to include velocities as high as 60  $\text{km s}^{-1}$ , thereby increasing the possibility of including emission from such flows. A cleaner

---

<sup>3</sup>Kwan’s theory of warm disk coronae has similarities with our X-ray irradiated disk atmospheres, but there are significant differences in the underlying ionization physics.

comparison case for our model might be provided by an X-ray bright star with a relatively low accretion rate, where the emission from outflows would be reduced.

Because TW Hya has a low mass-loss rate and a small accretion rate, it would be a good case for detailed modeling. Herczeg et al. (2007) detected the O I 6300/6363 Å lines in TW Hya at moderately high spectral resolution. The luminosity of the 6300 Å line,  $7.0 \times 10^{-6} L_{\odot}$ , is close to the result given in Table 3,  $8.0 \times 10^{-6} L_{\odot}$ , recalling the good agreement for the luminosity of the Ne II 12.81  $\mu\text{m}$  line. The 6300 Å line is centered on the stellar velocity, and it has a significantly narrower width than the Ne II line, but one that is still too large to be explained by pure rotational broadening. Again, interesting possible explanations to consider in future modeling are a turbulent atmosphere and photo-evaporation.

## 5.2. Low excitation lines

We next consider the low-excitation lines that arise from the fine-structure levels of O I (excitation energies 228 K and 327 K), C I (excitation energies 23.6 K and 62.5 K) and C II (excitation energy 91.2 K); they give rise to far-infrared emission at 63 and 145  $\mu\text{m}$  (O I), 609 and 370  $\mu\text{m}$  (C I), and 158  $\mu\text{m}$  (C II). Table 3 shows that the O I fine-structure lines are potential diagnostics of both the moderately warm, ionized gas produced by X-rays, and the cooler gas at large perpendicular column densities. As shown in Fig. 9, O I 63  $\mu\text{m}$  line emission extends down toward the mid-plane region, especially at small radial distances, due to the incomplete conversion of atomic oxygen into molecules and the relatively low excitation temperature of the  $J = 1 - 2$  transition.

The 63  $\mu\text{m}$  line has been observed around T Tauri stars with the KAO (e.g., Cohen et al. 1988; Ceccarelli et al. 1997) and ISO (e.g, Spinoglio et al. 2000; Creech-Eakman et al. 2002; Liseau et al. 2006). These observations were made with large beams (tens of arc seconds) and with moderate spatial resolution (50-300 km s<sup>-1</sup>). A typical flux for a T Tauri star in Taurus-Aurigae is quite large,  $\sim 10^{-12} - 10^{-11}$  erg cm<sup>-2</sup> s<sup>-1</sup>, and may include emission from other circumstellar material and not just disks. On the other hand, the flux calculations in Table 3 probably underestimate the flux, even though they integrate out to 100 AU, especially for the carbon lines. Jonkheid et al. (2004) have applied a code developed for (UV) photon-dominated regions to the surface layers of a flaring disk, and find that the fluxes of the O I, C I, and C II fine-structure lines are all of comparable brightness, and not that much weaker than the CO( $J = 1 - 0$ ) line. Photo-ionization of neutral carbon by external FUV radiation can enhance the abundance of C<sup>+</sup> and increase the flux of the C II 158  $\mu\text{m}$  line. Our model would have to be extended to include UV irradiation in order to get a fuller understanding of these low-excitation diagnostic lines.

Our estimate of the O I  $63\ \mu\text{m}$  line flux provides a good estimate of the emission of this line from the inner disk. Since its detection requires airborne or space observations, the identification with inner disk emission requires resolved line profiles and the assumption of Keplerian disk rotation. Such measurements could be made with heterodyne detectors aboard SOFIA or with *Herschel* (PACS).

## 6. Summary

We have used a simplified thermal-chemical and structural model to explore the diagnostics of the atomic gas in protoplanetary disks irradiated by stellar X-rays. Our focus has been on moderate disk radii out to roughly 25 AU, where stellar X-rays play an important role in ionizing and heating the upper layers of the disk. We find several diagnostics for this region, all of which arise from relatively high-excitation levels  $\sim 1000$  K: Ne II and Ne III fine-structure lines and O I, S II, and C I forbidden lines. Some low-excitation fine-structure lines are also of interest in the context of X-ray irradiation, especially the O I fine-structure lines, which generates strong disk emission over a substantial range of vertical column density, extending close to the mid-plane of the disk.

The atomic lines probe different depths of the disk at moderate radii. The forbidden transitions are generated at the top of the atmosphere, where the temperature and ionization levels are the highest. The mid-infrared fine-structure lines probe greater depths, where the temperature and ionization level have decreased. Neon is the cleanest case, since it does not easily form molecules, and its fine-structure lines originate from intermediate as well as top layers of the disk. On the other hand, the S I fine-structure lines are produced mainly in intermediate layers, since atomic sulfur has a low abundance in the top layers due to X-ray ionization and also near the mid plane, due to molecule formation. By contrast, the O I fine-structure lines are formed at almost all depths, including close to the mid plane, where the density is high and the upper levels of the transitions are more commensurate with the temperatures there.

The X-ray generated atomic lines discussed here are produced over a range of radii, extending from the inner radius of the disk out to 20-30 AU. To resolve these regions in nearby star-forming clusters at a nominal distance of 140 pc, requires a spatial resolution of  $\sim 0.1 - 0.2''$ , as well as resolved line profiles. For example, the Ne II  $12.81\ \mu\text{m}$  line should be detectable with TEXES or comparable spectrometers on large ground-based telescopes. A promising step in this direction is its detection with MICHELLE on Gemini North (Herczeg et al. 2007). The far-infrared lines of C I, C II, and O I will be detectable with instruments on board SOFIA and *Herschel*.

In presenting these results for a simplified T Tauri disk model irradiated by stellar X-rays, we have tried to mention and discuss its limitations. To summarize, there are, first of all, many uncertainties in the underlying atomic physics, such as missing rate coefficients for charge exchange with atomic hydrogen and for collisional excitation by abundant particles other than electrons. These uncertainties of course hold for all thermal-chemical/excitation models. Another limitation is the reliance on one type of disk, represented by the smooth density distribution of the generic T Tauri model of D’Alessio et al. (1999). Removing this restriction is one of our immediate goals. It will enable us to discuss disks of different ages and disks with non-monotonic density distributions such as holes, gaps, and rims. The improvements that are needed to treat situations such as disks with holes require a higher level model than used here. More generally, a 3-dimensional treatment is needed, and this dictates a greatly improved treatment of the radiation transfer, especially for the cooling lines and the external UV irradiation.

Focusing on X-rays to the exclusion of UV irradiation is another limitation that needs to be dealt with in future modeling. It is very likely that the well-documented X-rays produced by essentially all YSOs are the dominant external radiation source for radii less than 25 AU. At larger radii, however, ambient UV, from the general interstellar medium or from the host star cluster members, can affect disk properties. At smaller radii, UV radiation originating close to the star may also play a role, although it is more easily attenuated than moderately hard keV X-rays. We have ignored stellar UV radiation, which is poorly determined, in favor of the well-measured X-rays.

Granted that the X-rays likely play the dominant role within 25 AU or so, the relatively high-excitation transitions that they generate may be produced by some of the other dynamical components of the star-formation system that lie near and even inside the inner edge of the disk. The most obvious examples are the forbidden optical transitions produced by jets and accretion streams that are the signatures of actively accreting YSOs. In this situation, the high-excitation line strengths that we calculate for disks may only represent lower limits to those measured in spatially unresolved observations. A similar conclusion pertains to the low-excitation lines, where significant emission can arise from large disk radii where external UV can dominate. Of course the contributions of the various parts of the star formation complex can in principle be disentangled by observations with the appropriate spatial and spectral resolution, together with more complex models. The present results demonstrate the importance of X-ray irradiation in the ongoing process of elucidating the nature of the gas in protoplanetary disks.

## 7. Acknowledgements

This work has been supported by NSF Grant AST-0507423 and NASA Grant NNG06GF88G. We would like to express our appreciation to Dr. Javier Igea for his development of the thermal-chemical program used in this research. We would also like to thank Dr. Paola D’Alessio for providing the results of her disk model which form the basis of the calculations reported in this and previous publications.

## REFERENCES

- Abrahamsson, E., Krems, R. V., & Dalgarno, A. 2007, *ApJ*, 654, 1171
- Aldrovandi, S. M. V. & Pequignot, D. 1973, *A&A*, 25, 137
- Asplund, M., Grevesse, N., & Sauval, A. J. 2005, in *Astronomical Society of the Pacific Conference Series*, Vol. 336, *Cosmic Abundances as Records of Stellar Evolution and Nucleosynthesis*, ed. T. G. Barnes, III & F. N. Bash, 25–+
- Bahcall, J. N. & Wolf, R. A. 1968, *ApJ*, 152, 701
- Barinova, Ğ., van Hemert, M. C., Krems, R., & Dalgarno, A. 2005, *ApJ*, 620, 537
- Bergin, E. A., Aikawa, Y., Blake, G. A., & van Dishoeck, E. F. 2007, in *Protostars and Planets V*, ed. B. Reipurth, D. Jewitt, & K. Keil, 751–766
- Butler, K. & Zeippen, C. J. 1994, *A&AS*, 108, 1
- Butler, S. E. & Dalgarno, A. 1980, *ApJ*, 241, 838
- Calvet, N., Patino, A., Magris, G. C., & D’Alessio, P. 1991, *ApJ*, 380, 617
- Carr, J. S. 1989, *ApJ*, 345, 522
- Ceccarelli, C., Haas, M. R., Hollenbach, D. J., & Rudolph, A. L. 1997, *ApJ*, 476, 771
- Chambaud, G., Levy, B., Millie, P., Tran Minh, F., Launay, J. M., & Roueff, E. 1980, *Journal of Physics B Atomic Molecular Physics*, 13, 4205
- Chen, D., Gao, H., & Kwong, V. H. 2003, *Phys. Rev. A*, 68, 052703
- Chiang, E. & Murray-Clay, R. 2007, *Nature Physics*, 3, 604
- Christensen, R. B. & Watson, W. D. 1981, *Phys. Rev. A*, 24, 1331

- Cohen, M., Hollenbach, D. J., Haas, M. R., & Erickson, E. F. 1988, *ApJ*, 329, 863
- Creech-Eakman, M. J., Chiang, E. I., Joung, R. M. K., Blake, G. A., & van Dishoeck, E. F. 2002, *A&A*, 385, 546
- D’Alessio, P., Calvet, N., Hartmann, L., Lizano, S., & Cantó, J. 1999, *ApJ*, 527, 893
- Dullemond, C. P., Hollenbach, D., Kamp, I., & D’Alessio, P. 2007, in *Protostars and Planets V*, ed. B. Reipurth, D. Jewitt, & K. Keil, 555–572
- Dullemond, C. P., van Zadelhoff, G. J., & Natta, A. 2002, *A&A*, 389, 464
- Espaillet, C., Calvet, N., D’Alessio, P., Bergin, E., Hartmann, L., Watson, D., Furlan, E., Najita, J., Forrest, W., McClure, M., Sargent, B., Bohac, C., & Harrold, S. T. 2007, *ArXiv e-prints*, 707
- Feigelson, E. D., Getman, K., Townsley, L., Garmire, G., Preibisch, T., Grosso, N., Montmerle, T., Muench, A., & McCaughrean, M. 2005, *ApJS*, 160, 379
- Finocchi, F. & Gail, H.-P. 1997, *A&A*, 327, 825
- Florescu-Mitchell, A. I. & Mitchell, J. B. A. 2006, *Phys. Rep.*, 430, 277
- Font, A. S., McCarthy, I. G., Johnstone, D., & Ballantyne, D. R. 2004, *ApJ*, 607, 890
- Getman, K. V., Flaccomio, E., Broos, P. S., Grosso, N., Tsujimoto, M., Townsley, L., Garmire, G. P., Kastner, J., Li, J., Harnden, Jr., F. R., Wolk, S., Murray, S. S., Lada, C. J., Muench, A. A., McCaughrean, M. J., Meeus, G., Damiani, F., Micela, G., Sciortino, S., Bally, J., Hillenbrand, L. A., Herbst, W., Preibisch, T., & Feigelson, E. D. 2005, *ApJS*, 160, 319
- Glassgold, A. E. 1995, *ApJ*, 438, L111
- Glassgold, A. E., Najita, J., & Igea, J. 2004, *ApJ*, 615, 972
- Glassgold, A. E., Najita, J. R., & Igea, J. 2007, *ApJ*, 656, 515
- Goicoechea, J. R., Pety, J., Gerin, M., Teyssier, D., Roueff, E., Hily-Blant, P., & Baek, S. 2006, *A&A*, 456, 565
- Gorti, U. & Hollenbach, D. 2004, *ApJ*, 613, 424
- Gould, R. J. 1978, *ApJ*, 219, 250



- Griffin, D. C., Mitnik, D. M., & Badnell, N. R. 2001, *Journal of Physics B Atomic Molecular Physics*, 34, 4401
- Güdel, M., Briggs, K. R., Arzner, K., Audard, M., Bouvier, J., Feigelson, E. D., Franciosini, E., Glauser, A., Grosso, N., Micela, G., Monin, J.-L., Montmerle, T., Padgett, D. L., Palla, F., Pillitteri, I., Rebull, L., Scelsi, L., Silva, B., Skinner, S. L., Stelzer, B., & Telleschi, A. 2007, *A&A*, 468, 353
- Hartigan, P., Edwards, S., & Ghandour, L. 1995, *ApJ*, 452, 736
- Herczeg, G. J., Linsky, J. L., Valenti, J. A., Johns-Krull, C. M., & Wood, B. E. 2002, *ApJ*, 572, 310
- Herczeg, G. J., Najita, J., Hillenbrand, L. A., & Pascucci, I. 2007, *ArXiv e-prints*, 706
- Hirth, G. A., Mundt, R., & Solf, J. 1997, *A&AS*, 126, 437
- Hollenbach, D. & McKee, C. F. 1989, *ApJ*, 342, 306
- Hollenbach, D. J., Yorke, H. W., & Johnstone, D. 2000, *Protostars and Planets IV*, 401
- Igea, J. & Glassgold, A. E. 1999, *ApJ*, 518, 848
- Jaquet, R., Staemmler, V., Smith, M. D., & Flower, D. R. 1992, *Journal of Physics B Atomic Molecular Physics*, 25, 285
- Jonkheid, B., Dullemond, C. P., Hogerheijde, M. R., & van Dishoeck, E. F. 2007, *A&A*, 463, 203
- Jonkheid, B., Faas, F. G. A., van Zadelhoff, G.-J., & van Dishoeck, E. F. 2004, *A&A*, 428, 511
- Jonkheid, B., Kamp, I., Augereau, J.-C., & van Dishoeck, E. F. 2006, *A&A*, 453, 163
- Kamp, I., van Zadelhoff, G.-J., van Dishoeck, E. F., & Stark, R. 2003, *A&A*, 397, 1129
- Kastner, J. H., Huenemoerder, D. P., Schulz, N. S., Canizares, C. R., & Weintraub, D. A. 2002, *ApJ*, 567, 434
- Krems, R. V., Jamieson, M. J., & Dalgarno, A. 2006, *ApJ*, 647, 1531
- Kwan, J. 1997, *ApJ*, 489, 284
- Kwan, J. & Tadamaru, E. 1988, *ApJ*, 332, L41

- . 1995, *ApJ*, 454, 382
- Lahuis, F., van Dishoeck, E. F., Blake, G. A., Evans, II, N. J., Kessler-Silacci, J. E., & Pontoppidan, K. M. 2007, *ArXiv e-prints*, 704
- Launay, J. M. & Roueff, E. 1977a, *A&A*, 56, 289
- Launay, J.-M. & Roueff, E. 1977b, *Journal of Physics B Atomic Molecular Physics*, 10, 879
- Leen, T. M. & Graff, M. M. 1988, *ApJ*, 325, 411
- Liseau, R., Justtanont, K., & Tielens, A. G. G. M. 2006, *A&A*, 446, 561
- Maloney, P. R., Hollenbach, D. J., & Tielens, A. G. G. M. 1996, *ApJ*, 466, 561
- Millar, T. J. & Herbst, E. 1990, *A&A*, 231, 466
- Monteiro, T. S. & Flower, D. R. 1987, *MNRAS*, 228, 101
- Nahar, S. N. & Pradhan, A. K. 1995, *ApJ*, 447, 966
- Najita, J., Carr, J. S., & Mathieu, R. D. 2003, *ApJ*, 589, 931
- Najita, J. R., Carr, J. S., Glassgold, A. E., & Valenti, J. A. 2007, in *Protostars and Planets V*, ed. B. Reipurth, D. Jewitt, & K. Keil, 507–522
- Najita, J. R., Edwards, S., Basri, G., & Carr, J. 2000, *Protostars and Planets IV*, 457
- Nisini, B., Benedettini, M., Giannini, T., Caux, E., di Giorgio, A. M., Liseau, R., Lorenzetti, D., Molinari, S., Saraceno, P., Smith, H. A., Spinoglio, L., & White, G. J. 1999, *A&A*, 350, 529
- Pascucci, I., Hollenbach, D., Najita, J., Muzerolle, J., Gorti, U., Herczeg, G. J., Hillenbrand, L. A., Kim, J. S., Carpenter, J. M., Meyer, M. R., Mamajek, E. E., & Bouwman, J. 2007, *ArXiv Astrophysics e-prints*
- Pequignot, D. 1990, *A&A*, 231, 499
- Pequignot, D. & Aldrovandi, S. M. V. 1976, *A&A*, 50, 141
- Pudritz, R. E., Ouyed, R., Fendt, C., & Brandenburg, A. 2007, in *Protostars and Planets V*, ed. B. Reipurth, D. Jewitt, & K. Keil, 277–294
- Ray, T., Dougados, C., Bacciotti, F., Eisloffel, J., & Chrysostomou, A. 2007, in *Protostars and Planets V*, ed. B. Reipurth, D. Jewitt, & K. Keil, 231–244

- Savage, B. D. & Sembach, K. R. 1996, *ARA&A*, 34, 279
- Spinoglio, L., Giannini, T., Nisini, B., van den Ancker, M. E., Caux, E., Di Giorgio, A. M., Lorenzetti, D., Palla, F., Pezzuto, S., Saraceno, P., Smith, H. A., & White, G. J. 2000, *A&A*, 353, 1055
- Stelzer, B. & Schmitt, J. H. M. M. 2004, *A&A*, 418, 687
- Stepinski, T. F. 1992, *Icarus*, 97, 130
- Störzer, H. & Hollenbach, D. 2000, *ApJ*, 539, 751
- Tayal, S. S. 1997, *ApJS*, 111, 459
- . 2004, *ApJS*, 153, 581
- Telleschi, A., Güdel, M., Briggs, K. R., Audard, M., & Palla, F. 2007, *A&A*, 468, 425
- Uchida, K. I., Calvet, N., Hartmann, L., Kemper, F., Forrest, W. J., Watson, D. M., D’Alessio, P., Chen, C. H., Furlan, E., Sargent, B., Brandl, B. R., Herter, T. L., Morris, P., Myers, P. C., Najita, J., Sloan, G. C., Barry, D. J., Green, J., Keller, L. D., & Hall, P. 2004, *ApJS*, 154, 439
- Umebayashi, T. & Nakano, T. 1981, *PASJ*, 33, 617
- Wilson, N. J. & Bell, K. L. 2002, *MNRAS*, 337, 1027
- Wolk, S. J., Harnden, Jr., F. R., Flaccomio, E., Micela, G., Favata, F., Shang, H., & Feigelson, E. D. 2005, *ApJS*, 160, 423
- Zatsarinny, O., Bartschat, K., Bandurina, L., & Gedeon, V. 2005, *Phys. Rev. A*, 71, 042702
- Zatsarinny, O. & Tayal, S. S. 2003, *ApJS*, 148, 575
- Zhao, L. B., Stancil, P. C., Gu, J.-P., Liebermann, H.-P., Funke, P., Buenker, R. J., & Kimura, M. 2005, *Phys. Rev. A*, 71, 062713

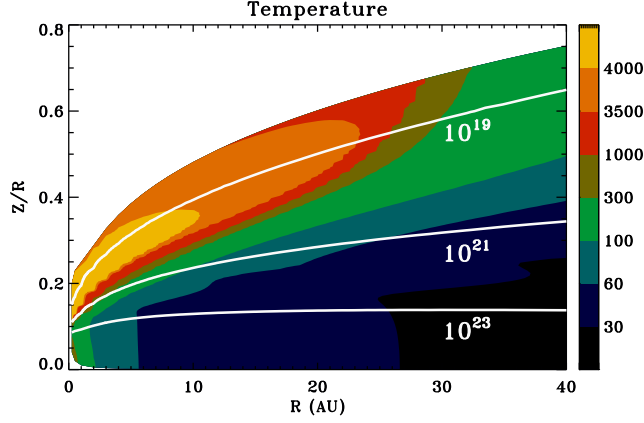


Fig. 1.— Gas temperature structure of the reference model described in the text with color code on the right. The density structure is based on the D’Alessio et al. (1999) model, defined by the parameters:  $M_* = 0.5M_\odot$ ,  $R = 2R_\odot$ ,  $T_* = 4000$  K,  $\dot{M} = 10^{-8} M_\odot \text{yr}^{-1}$ . The reference X-ray luminosity is  $L_X = 2 \times 10^{30} \text{ erg s}^{-1}$ , and the temperature of the thermal X-ray spectrum is  $kT_X = 1$  keV. The white curves are contours of fixed vertical column density  $N_H$  in units of  $\text{cm}^{-2}$ . The curve for  $N_H = 10^{21} \text{ cm}^{-2}$  corresponds roughly to two scale heights as defined near the mid-plane. The integrated surface density varies roughly as  $1/R$  for  $R > 1$  AU and somewhat less rapidly for  $R < 1$  AU.

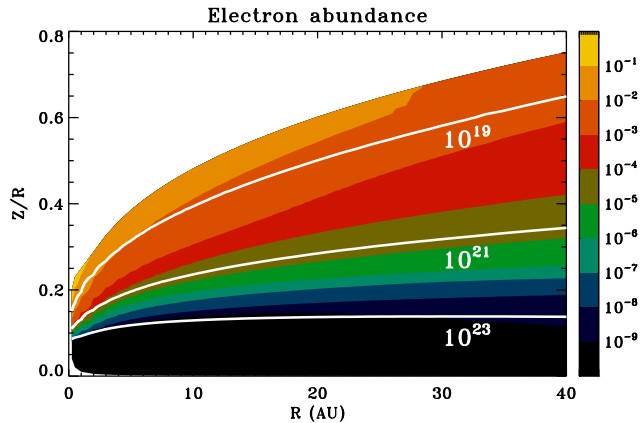


Fig. 2.— Spatial distribution of the electron fraction plotted in the same way as Fig. 1, except for the color-coded units.

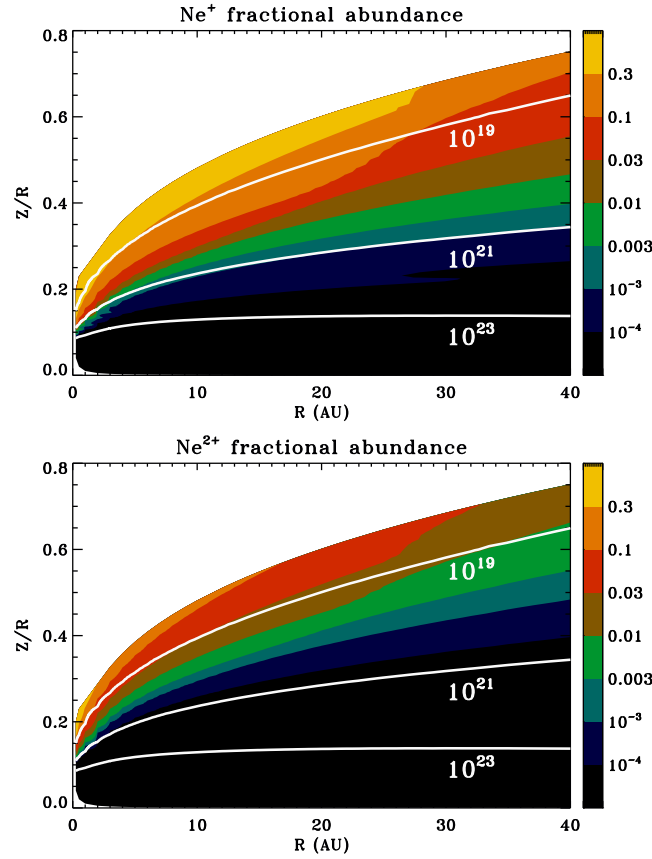


Fig. 3.— Spatial distribution of the  $\text{Ne}^+$  and  $\text{Ne}^{2+}$  abundances relative to the total abundance of neon, plotted in the same way as Figure 1.

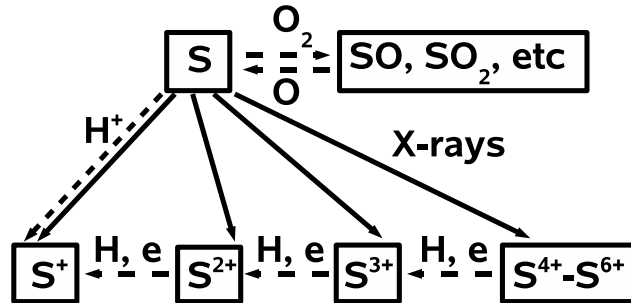


Fig. 4.— Schematic diagram of sulfur chemistry. Charge exchange of sulfur ions with hydrogen atoms is critical for the ionization structure at high altitudes, whereas molecule formation controls the abundance of atomic sulfur near the mid-plane.

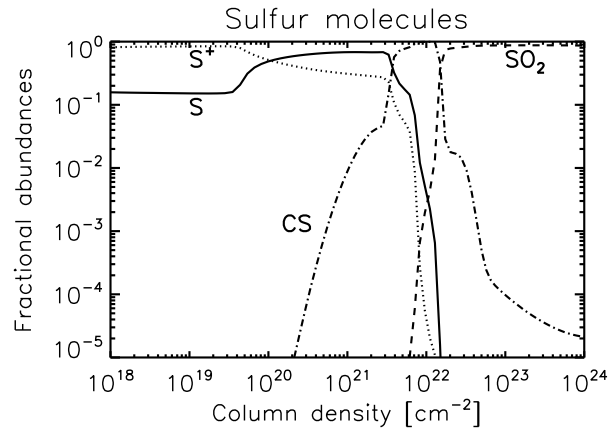


Fig. 5.— Fractional sulfur abundances vs. vertical column density measured from the top of disk at a radial distance of 20 AU from the star.  $\text{SO}_2$  becomes the dominant species at large columns.

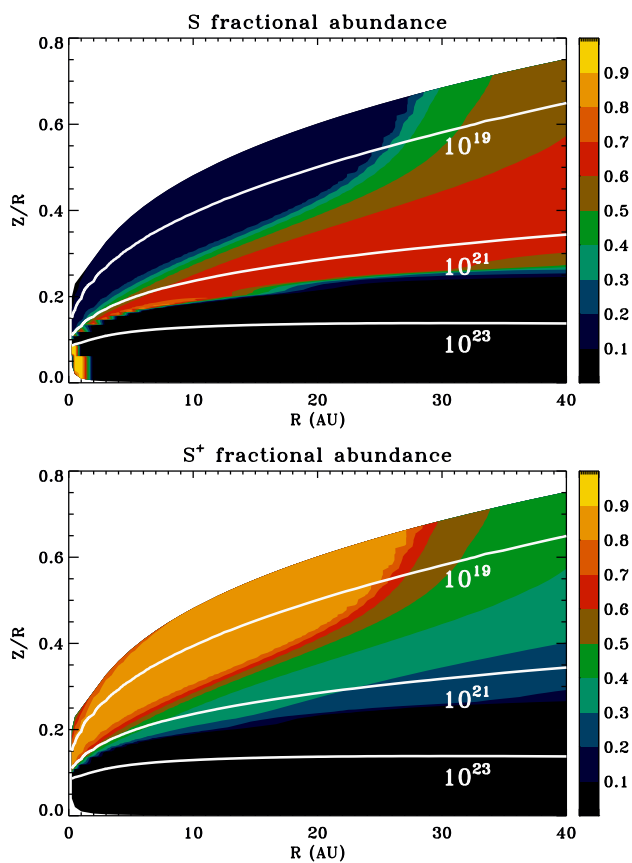


Fig. 6.— Spatial distribution of normalized S and S<sup>+</sup> abundances, plotted in the manner of Figure 1.

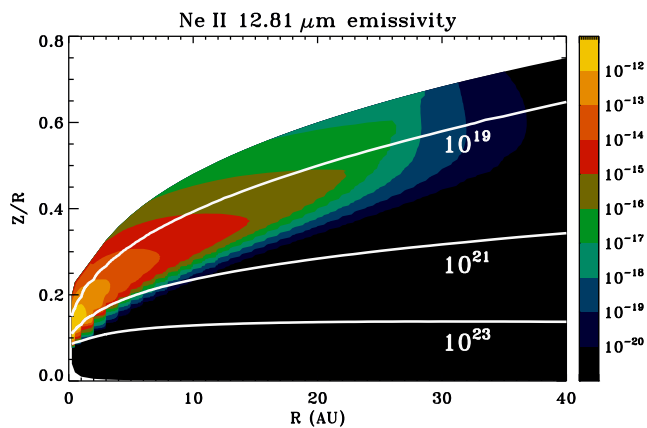


Fig. 7.— The spatial variation of the Ne II 12.81  $\mu\text{m}$  fine structure emissivity, defined by equation (1), in units of  $\text{erg cm}^{-3}\text{s}^{-1}$ .

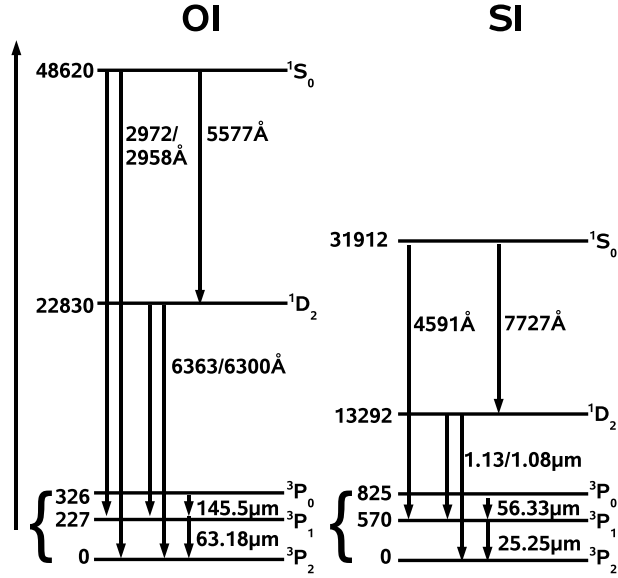


Fig. 8.— Energy level diagrams for O and S showing the low-lying levels that generate the fine-structure and forbidden lines. Note that the energy scale is in Kelvin.

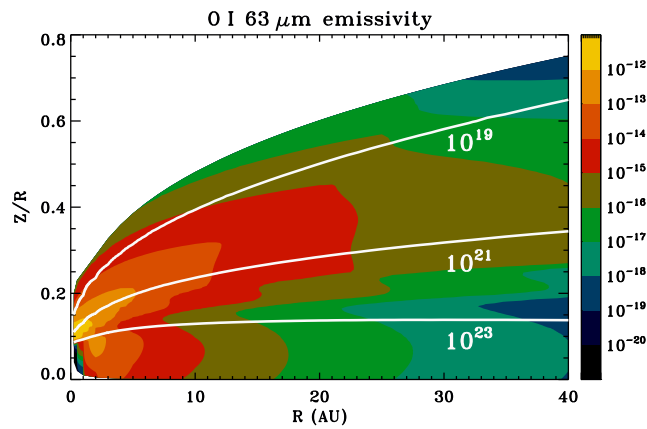


Fig. 9.— Spatial distribution of the O I 63 μm fine-structure line emissivity, defined by equation (1), in units of  $\text{erg cm}^{-3} \text{s}^{-1}$ .



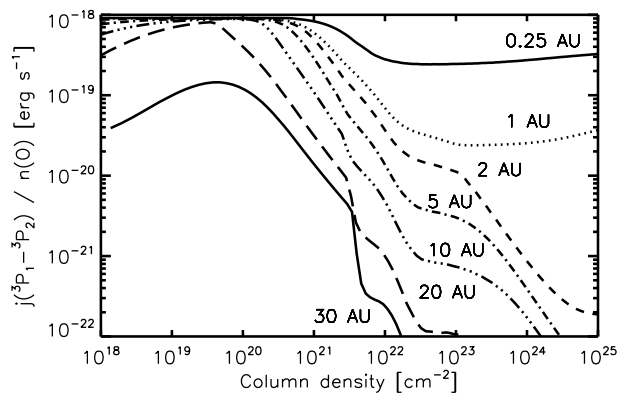


Fig. 10.— The specific O I  $63\ \mu\text{m}$  emissivity in units of  $\text{erg s}^{-1} \text{atom}^{-1}$ , vs. perpendicular column density at various radii.

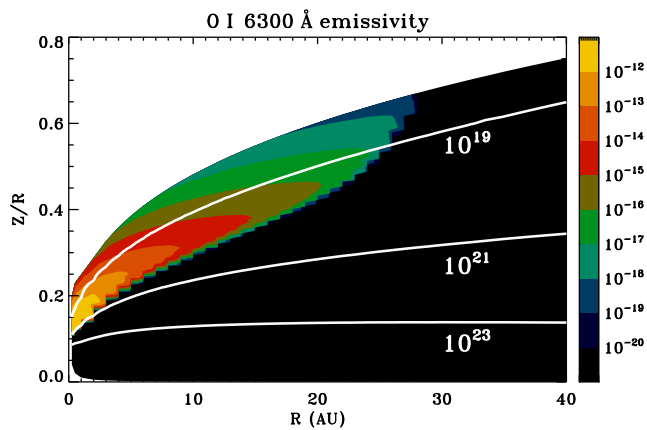


Fig. 11.— Spatial distribution of the O I  $6300\ \text{\AA}$  forbidden line emissivity, in units of  $\text{erg cm}^{-3} \text{s}^{-1}$ .

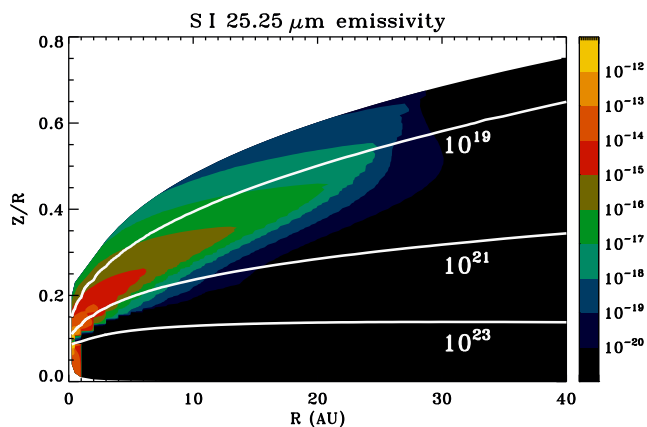


Fig. 12.— Spatial distribution of the SI 25.55  $\mu\text{m}$  fine-structure line emission in units of  $\text{erg cm}^{-3} \text{s}^{-1}$ . The emission peaks at intermediate depths, as discussed in the text.

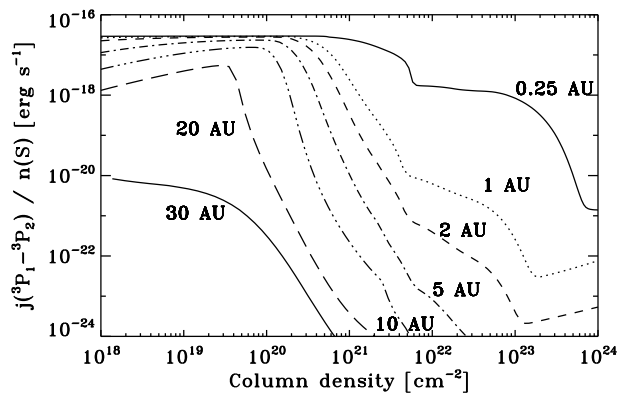


Fig. 13.— The spatial distribution of the specific emissivity in units of  $\text{erg cm}^{-3} \text{s}^{-1} \text{atom}^{-1}$  of the SI 25.55  $\mu\text{m}$  fine-structure line vs. perpendicular column density at several radii.

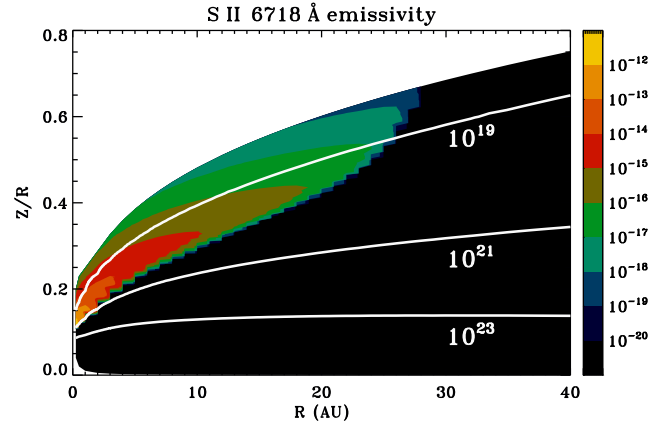


Fig. 14.— Spatial distribution of the S II 6718 Å forbidden line emission in units of  $\text{erg cm}^{-3} \text{s}^{-1}$ . Significant emission only occurs in the warmest part of the disk atmosphere.

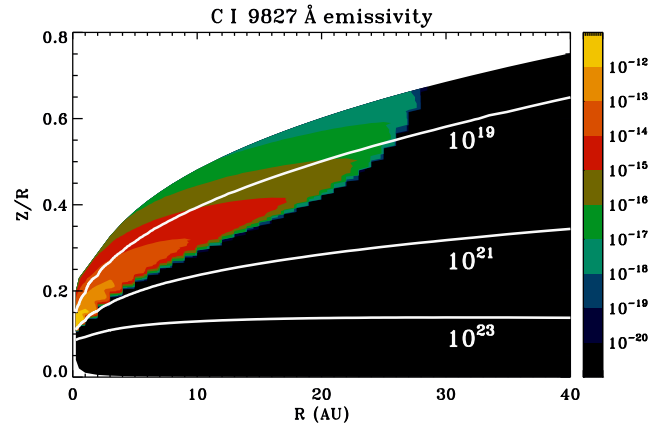


Fig. 15.— Spatial distribution of the C I forbidden line emission in units of  $\text{erg cm}^{-3} \text{s}^{-1}$ .

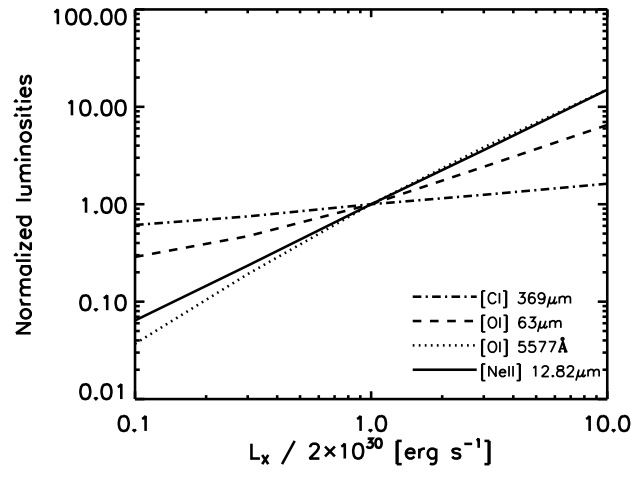


Fig. 16.— The variation of selected line fluxes with X-ray luminosity, all normalized to the values for the reference model.

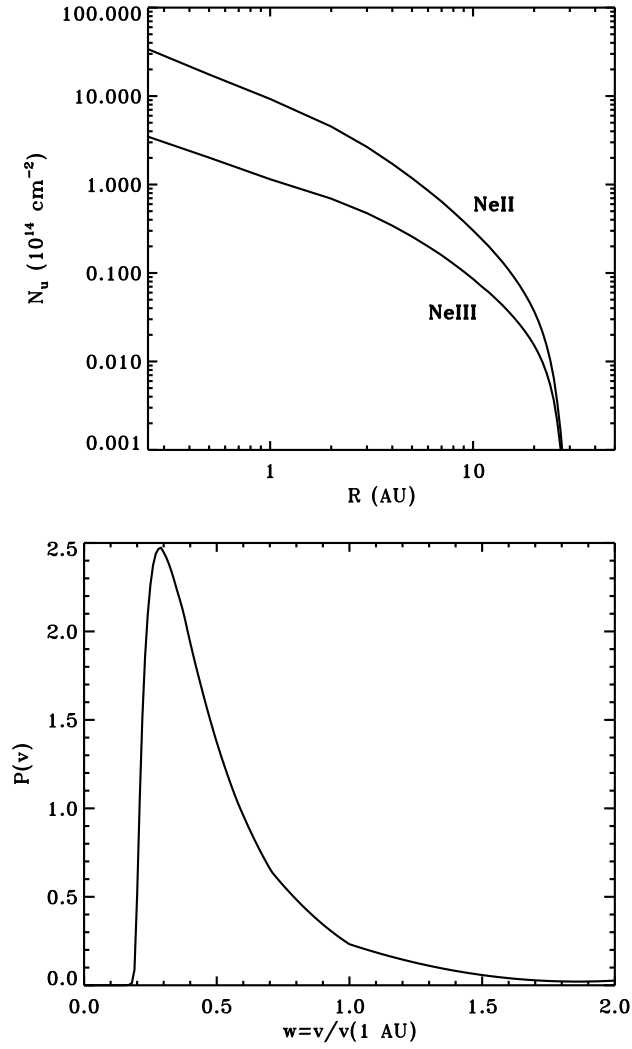


Fig. 17.— Column densities of excited Ne ions in units of  $10^{14} \text{ cm}^{-2}$  plotted vs. radial distance in AU (left), and the rotational velocity distribution function  $P(v)$  plotted vs. velocity normalized to its value at 1 AU (right).

Table 1: Selected Reaction Rate coefficients for Sulfur

Reactants	Products	Symbol	Rate coefficient	Reference
$S^+ + e$	$S + h\nu$	$\alpha_1$	$4.65 \times 10^{-13} T_4^{-0.63}$	Aldrovandi & Pequignot (1973); Gould (1978)
$S^{2+} + e$	$S^+ + h\nu$	$\alpha_2$	$3.37 \times 10^{-12} T_4^{-0.50}$	Nahar & Pradhan (1995)
$S^{3+} + e$	$S^{2+} + h\nu$	$\alpha_3$	$5.23 \times 10^{-12} T_4^{-0.50}$	Nahar & Pradhan (1995)
$H^+ + S$	$S^+ + H$	$k_1$	$5 \times 10^{-12*}$	Zhao et al. (2005)
$S^+ + H$	$H^+ + S$	$k_1$	negligible	Zhao et al. (2005)
$S^{2+} + H$	$H^+ + S^+$	$k_2$	$10^{-14}$	Butler & Dalgarno (1980); Christensen & Watson (1981)
$S^{3+} + H$	$H^+ + S^{2+}$	$k_3$	$3 \times 10^{-9}$	Butler & Dalgarno (1980); Christensen & Watson (1981)
$S^{2+} + H_2$	S etc.	$BK$	$2 \times 10^{-9}B$	Chen et al. (2003)
$S^{2+} + H_2$	$S^+$ etc.	$(1 - B)K$	$2 \times 10^{-9}(1-B)$	Chen et al. (2003)
S+ X-ray	$S^+ + e$	$\zeta_{\text{sec}}(S)$	$5 \times \zeta$	This work.
S+ X-ray	$S^{2+} + 2e$	$\zeta_{\text{dir}}(S)$	$20 \times \zeta$	This work.
$S^+ + X\text{-ray}$	$S^{2+} + e$	$\zeta(S)$	$25 \times \zeta$	This work.

\* Approximate value valid from 500-5,000 K

Table 2: References for excitation coefficients\*

Ion	references
NeII fine structure	Griffin et al. (2001) (e)
NeIII fine structure	Butler & Zeippen (1994) (e)
O I fine structure	Launay & Roueff (1977a); Abrahamsson et al. (2007) (H); Jaquet et al. (1992) (H <sub>2</sub> ); Monteiro & Flower (1987) (He); Chambaud et al. (1980) (p); Pequignot (1990) (e)
O I forbidden	Krems et al. (2006) (H); Zatsarinny & Tayal (2003) (e)
SI fine structure	Tayal (2004) (e)
SII forbidden	Tayal (1997) (e)
CI fine structure	Launay & Roueff (1977a); Abrahamsson et al. (2007) (H); Monteiro & Flower (1987) (He, H <sub>2</sub> )
CI forbidden	Pequignot & Aldrovandi (1976); Zatsarinny et al. (2005) (e)
CII fine structure	Barinovs et al. (2005) (H); Launay & Roueff (1977b) (H <sub>2</sub> ); Wilson & Bell (2002) (e)

\*The collision partners are specified inside the brackets.

Table 3: Unresolved line fluxes in  $\text{erg s}^{-1} \text{cm}^{-2}$ \*

$L_X$ ( $\text{erg s}^{-1}$ )	$2.0 \times 10^{29}$	$6.0 \times 10^{29}$	<b><math>2.0 \times 10^{30}</math></b>	$6.0 \times 10^{30}$	$2.0 \times 10^{31}$
Ne II $12.82 \mu\text{m}$	$4.1 \times 10^{-16}$	$1.5 \times 10^{-15}$	<b><math>6.4 \times 10^{-15}</math></b>	$2.3 \times 10^{-14}$	$9.6 \times 10^{-14}$
Ne III $15.55 \mu\text{m}$	$3.0 \times 10^{-17}$	$1.4 \times 10^{-16}$	<b><math>7.4 \times 10^{-16}</math></b>	$3.3 \times 10^{-15}$	$1.7 \times 10^{-14}$
O I $63 \mu\text{m}$	$1.9 \times 10^{-14}$	$3.1 \times 10^{-14}$	<b><math>6.6 \times 10^{-14}</math></b>	$1.6 \times 10^{-13}$	$4.3 \times 10^{-13}$
O I $146 \mu\text{m}$	$9.6 \times 10^{-16}$	$1.2 \times 10^{-15}$	<b><math>1.8 \times 10^{-15}</math></b>	$3.8 \times 10^{-15}$	$1.1 \times 10^{-14}$
O I $6300 \text{ \AA}^{**}$	$1.1 \times 10^{-15}$	$3.6 \times 10^{-15}$	<b><math>1.3 \times 10^{-14}</math></b>	$4.5 \times 10^{-14}$	$1.7 \times 10^{-13}$
O I $5577 \text{ \AA}$	$2.7 \times 10^{-17}$	$1.4 \times 10^{-16}$	<b><math>7.3 \times 10^{-16}</math></b>	$2.8 \times 10^{-15}$	$1.1 \times 10^{-14}$
Si I $25.25 \mu\text{m}$	$7.0 \times 10^{-17}$	$1.3 \times 10^{-16}$	<b><math>3.4 \times 10^{-16}</math></b>	$9.5 \times 10^{-16}$	$3.1 \times 10^{-15}$
Si I $56.23 \mu\text{m}$	$6.4 \times 10^{-18}$	$9.0 \times 10^{-18}$	<b><math>1.7 \times 10^{-17}</math></b>	$4.0 \times 10^{-17}$	$1.2 \times 10^{-16}$
S II $6718 \text{ \AA}$	$4.1 \times 10^{-17}$	$1.7 \times 10^{-16}$	<b><math>8.3 \times 10^{-16}</math></b>	$3.5 \times 10^{-15}$	$1.6 \times 10^{-14}$
S II $6733 \text{ \AA}$	$9.2 \times 10^{-18}$	$3.9 \times 10^{-17}$	<b><math>2.0 \times 10^{-16}</math></b>	$8.6 \times 10^{-16}$	$4.2 \times 10^{-15}$
C II $158 \mu\text{m}$	$1.2 \times 10^{-18}$	$3.2 \times 10^{-18}$	<b><math>9.8 \times 10^{-18}</math></b>	$2.8 \times 10^{-17}$	$9.0 \times 10^{-17}$
CI $369 \mu\text{m}$	$9.8 \times 10^{-16}$	$1.2 \times 10^{-15}$	<b><math>1.6 \times 10^{-15}</math></b>	$2.0 \times 10^{-15}$	$2.6 \times 10^{-15}$
CI $609 \mu\text{m}$	$3.2 \times 10^{-16}$	$3.8 \times 10^{-16}$	<b><math>4.5 \times 10^{-16}</math></b>	$5.4 \times 10^{-16}$	$6.4 \times 10^{-16}$
CI $9827 \text{ \AA}^{**}$	$3.5 \times 10^{-16}$	$1.4 \times 10^{-15}$	<b><math>6.3 \times 10^{-15}</math></b>	$2.5 \times 10^{-14}$	$1.1 \times 10^{-13}$

\* A nominal distance of 140 pc has been assumed. Luminosities can be obtained by multiplying by  $4\pi(140\text{pc})^2 = 2.35 \times 10^{42} \text{cm}^2$ . The middle column refers to the reference model.

\*\* The O I  $6363 \text{ \AA}$  and CI  $9853 \text{ \AA}$  fluxes can be obtained by multiplying the fluxes of O I  $6300 \text{ \AA}$  by 0.244 and CI  $9827 \text{ \AA}$  by 0.248, respectively.